第33卷 第2期 焊 接 学 报 Vol. 33 No. 2
2012年2月 TRANSACTIONS OF THE CHINA WELDING INSTITUTION February 2012

激光熔覆 Fe-W 合金涂层的组织及性能

武 扬，虞 钢，何秀丽，宁伟健
(中国科学院力学研究所 先进制造工艺力学实验室，北京 100190)

武 扬

摘 要：以纯钨粉末为熔覆材料，采用同轴送粉激光熔覆技术，在Q235A钢表面制备了Fe-W合金耐磨涂层. 利用X射线衍射(XRD)、光学显微镜、扫描电镜(SEM)及能谱(EDS)对熔覆层的显微组织进行了分析，用显微硬度计和摩擦磨损试验机对熔覆层的硬度和耐磨性进行了测试. 结果表明，熔覆层与基底冶金结合，无明显裂纹或气孔，涂层内部由致密的粗大树枝状和短棒状 Fe_7W_6 增强相以及弥散分布的细小颗粒状 Fe_2W 相组成，其均匀分布在 α-Fe 固溶体中. 熔覆层平均硬度700 HV，为基材Q235A钢的3.5倍，同时耐磨性能也得到了显著提高.

关键词：激光熔覆；同轴送粉；Fe-W合金涂层；显微硬度；耐磨性
中图分类号：TG146.4；TN249 **文献标识码**：A **文章编号**：0253-360X(2012)02-0037-04

0 序 言

在工程、建筑、船舶、矿山开采等领域中，低碳低合金结构钢使用广泛，其在服役过程中往往面临着剧烈冲击和高磨损环境，这对零件强度、耐磨、疲劳寿命等性能提出了苛刻要求. 零件的磨损等破坏都是从表面开始的，因此在表面施加综合性能优异的保护涂层成为目前提高此类零件性能的重要方法.

激光熔覆是一种先进的表面涂层技术，熔覆材料在激光作用下熔化，与基体表面相熔合形成冶金结合熔覆层，可明显改善零件的表面性能或赋予其新的特性，具有广泛的应用前景[1]. 在利用激光熔覆技术提高钢材表面性能方面已开展了相关研究，如通过调整粉末配方在45钢表面获得激光熔覆TiC-Mo_2C陶瓷涂层[2]，采用激光熔覆技术在低碳钢表面制备Fe-B系原位自生颗粒增强铁基复合涂层来提高钢表面硬度[3,4]，以及激光熔覆高温合金涂层提高不锈钢磨损及热腐蚀性能[5]等. 钨作为常用难熔金属之一具有高熔点、高硬度、耐腐蚀等特性，使得钨及其化合物具有优异的应用价值[6,7]. 铁对钨具有很好的润湿性，铁和钨形成的Fe-W合金具有良好的硬度和耐磨性. 合金中的钨对钢起到强化作用，可在不明显降低钢塑性的情况下提高钢的强度极限和屈服点. 钨粉末容易获得，但纯钨粉末颗粒尺寸及形状不可控加之钨本身具有熔点高、比重大、高温易氧化等特性，用于激光熔覆加工存在一定困难，研究较少，在激光熔覆Fe-W合金涂层方面未见相关报道.

文中采用同轴送粉激光熔覆方法，以纯钨粉末为熔覆材料，Q235A钢为基底，针对工艺难点改进激光熔覆装置，优化工艺参数后在Q235A钢表面熔覆生成Fe-W合金耐磨涂层，对该难熔合金熔覆层的组织成分及性能进行了研究.

1 试验方法

试验中基底采用尺寸为100 mm×50 mm×10 mm的Q235A钢板，使用前对基底进行磨光，并用丙酮和无水乙醇进行清洗. 熔覆材料为纯钨粉末，粉末尺寸和形貌如图1所示. 由图1可以看出，粉末平均粒度<2 μm，形状不规则，为保证粉末输送过程的流畅性，使用前进行筛分处理，并在90 ℃下烘干6 h.

试验使用Nd:YAG固体激光器，采用同轴送粉多道搭接、逐层堆积形成熔覆层. 具体参数为激光功率1 000 W，离焦量15 mm，扫描速度1 mm/s，层高0.1 mm，搭接率50%，送粉率1 g/min，熔覆层数20，氩气保护.

采用Rigaku Dmax-RB X射线衍射仪(XRD)对熔覆层进行物相分析，利用NephotII光学金相显微镜和ZEISS EVO18 Special Edition扫描电镜(SEM)以及BRUKER Nano XFlash Detector 5010能谱仪

收稿日期：2010-12-06
基金项目：国家自然科学基金重点资助项目(10832011)

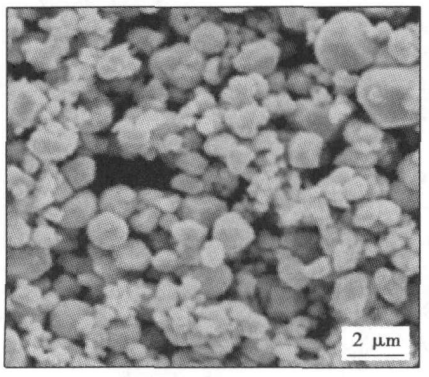

图 1 纯钨粉末颗粒形貌

Fig. 1 Morphology of tungsten powder particles

(EDS) 分析熔覆层显微组织成分. 利用 HXD-1000B 电子显微硬度计测量熔覆层硬度,载荷 0.1 N,加载保持时间 15 s.

在室温下,采用 M-200 型环块式磨损试验机进行磨损试验,试验所采用的磨损环材料为 GCr15,硬度为 64 HRC,环形直径为 48 mm,宽度为 13 mm,磨损时设定载荷为 100 N,摩擦轮转速为 140 r/min. 磨损前后在 Sartorius BP211D 电子天平上称取试样质量,以磨损失重比较原始基材和激光熔覆涂层的耐磨性能.

2 试验结果

2.1 激光熔覆显微组织

激光熔覆层截面方向组织结构如图 2 所示. 由图 2 可以看出熔覆层与基底形成了良好的冶金结合,没有明显的裂纹或气孔. 采用送粉式激光熔覆的涂层增长速度较慢,在激光束的往复作用下,已形成的熔覆层会受到激光的二次辐照,其中表层部分再次熔化与新输入的熔覆材料一起重新凝固形成新熔覆层. 试验中经过 20 层堆积后的熔覆层厚度约为 2 mm,可以推断平均层高为 100 μm,考虑重熔部分,加工中单次熔深约为 150 μm. 熔覆层沿截面方向分为明暗不同的三个区域: 熔覆层上部的灰白色区域位于基底水平线以上,该区域熔覆材料与基底材料的扩散作用相对较弱,为组织稳定生长的熔覆区(CZ);在熔覆区下方的浅灰色区域中,基材熔化较多,稀释作用较强形成了稀释区(DZ);稀释区与熔覆层熔合线之间还存在一个较薄的深灰色区域,该区域主要是熔覆初期熔池温度较低致使反应不够充分而形成的界面区(BZ);熔合线以下依次为热影响区(HAZ) 和基底原始材料.

熔覆层 X 射线衍射分析(XRD) 结果如图 3 所示. 由衍射图谱可以看出,熔覆层的主要成分为 α-Fe,Fe_7W_6,Fe_2W 和 W. 表明通过激光熔覆,熔覆材料与基底材料发生化合反应,在基底表面形成了 Fe-W 合金涂层.

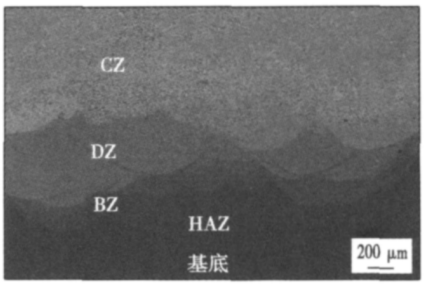

图 2 熔覆层显微组织

Fig. 2 Microstructure of clad layer

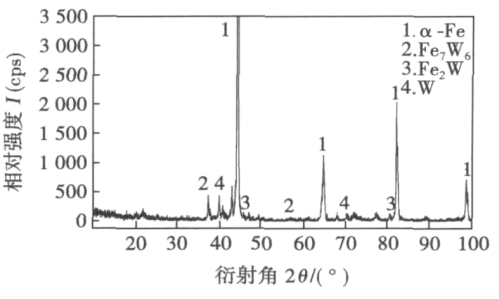

图 3 熔覆层 X 射线衍射图谱

Fig. 3 XRD spectrum of clad layer

2.2 激光熔覆层显微硬度及磨损性能

图 4 所示为熔覆层表面至基底截面方向的显微硬度曲线,可以看出从熔覆层至基底硬度值呈下降趋势,各区域的显微硬度有所不同. 熔覆层中熔覆区的硬度最高,但有较大的不均匀性,其硬度值 HV0.1 在 650 ~ 800 之间,局部硬度可高达 1 000 以上,平均硬度约为基体的 3.5 倍. 稀释区的硬度平均为 450 HV,界面区的硬度在 250 ~ 300 HV 之间,热影响区的硬度平均为 210 HV,略高于基底的平均硬度(200 HV).

图 5 所示为熔覆层和基体材料的磨损试验曲线. 结果表明,激光熔覆 Fe-W 合金熔覆层具有优良的耐磨性,与原始 Q235A 钢相比提高约 4 倍. 图 6 所示为基底和熔覆层磨损后的表面形貌,可以看出磨损后的基体表面出现了很多深的沟槽,并伴有大面积的脱落现象,说明基体材料在摩擦副作用下发生塑性变形而导致剥离,摩擦过程以粘着磨损为主. 相比之下熔覆层表面磨损后形貌较为平整,没有明显的沟壑,仅局部存在少量的凹坑,磨损过程表现为

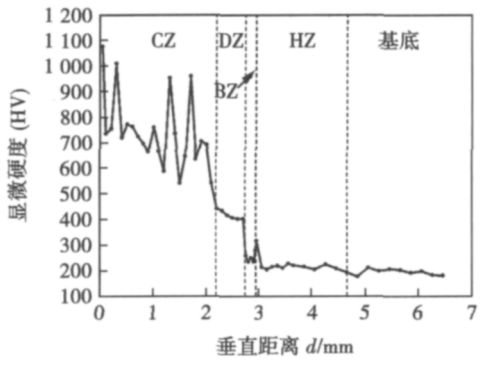

图 4　激光熔覆层沿层深方向显微硬度

Fig. 4　Microhardness of laser-clad coating as function of distance from surface

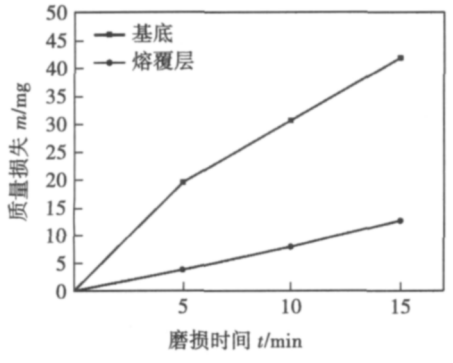

图 5　基底和熔覆层磨损曲线

Fig. 5　Weight loss at different time intervals during wear test

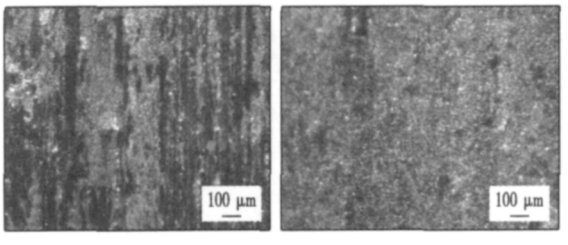

图 6　摩擦磨损表面形貌

Fig. 6　Worn surface of substrate and clad layer

磨粒磨损形式.

3　分析与讨论

激光熔覆过程中钨粉颗粒在下落过程中进入激光束,吸收激光能量熔化,剩余能量直接照射在基材上,使基材表面熔化形成熔池. 熔化的粉末液滴与部分未完全熔化的较大颗粒一起进入基底熔池混合. 由于 W 元素比重较大,在熔池中会趋向熔池底部流动,而 Fe 元素则倾向熔池上方浮动,密度差异有利于元素充分扩散. 此外之前未完全熔化的粉末颗粒可以吸收熔池热量进一步熔化,最终在基底表面形成含有 Fe 和 W 元素的合金熔池. 由于激光熔覆冷却速度极快,发生非平衡凝固形成熔覆层.

熔覆层截面各区域的 SEM 显微组织如图 7 所示,图 7 中各区域 EDS 结果如表 1,图 7a ~ 图 7d 矩形框为能谱区域面扫描范围. 图 7a 所示为熔覆层熔合线上方界面区组织形貌. 由 EDS 结果可知该区域 Fe 元素比例接近 90%,说明界面区主要为重熔的基体材料,而其内部分散的白色细小颗粒的成分

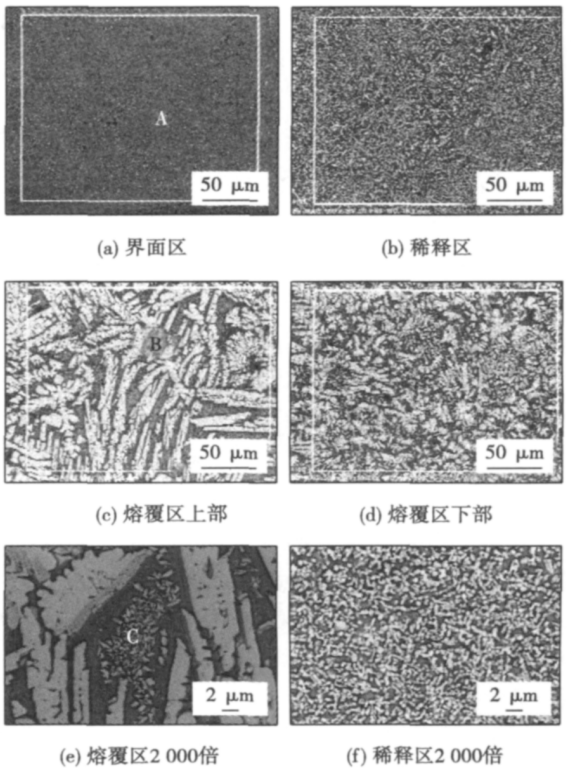

图 7　熔覆层不同位置 SEM 显微组织形貌

Fig. 7　SEM micrograph showing microstructure of laser-clad coating

表 1　激光熔覆层各区域 EDS 分析结果

Table 1　EDS analysis of laser-clad coating

		W	Fe	总量
点分布	A	71.21	28.79	100.00
	B	65.78	34.22	100.00
	C	46.70	53.30	100.00
区域分布	BZ	11.61	88.39	100.00
	DZ	40.27	59.73	100.00
	U-CZ	55.57	44.43	100.00
	L-CZ	50.83	49.17	100.00

主要为钨,结合 XRD 结果可以推断其为钨单质. 这是由于在熔覆初始阶段,激光照射时间短,基底温度低,热扩散作用强,导致基底表面的熔池温度较低,不足以充分熔化尺寸较大的粉末颗粒,激光束移动过后熔池快速冷却凝固,这些未熔颗粒就以单质形式被保留其中.

随着熔覆过程进行,基底和熔池不断吸收热量温度升高,同时在激光束作用下,熔池内液体产生强烈对流,使熔覆材料和基底材料充分混合. 在接近基底的区域,熔池内含有较多的 Fe 元素,凝固后形成稀释区(DZ) ,其组织为图 7b 所示的致密白灰色细小颗粒相. 根据 Fe-W 二元相图,在富含 Fe 元素的区域,1 548 ℃时固溶体 α-Fe 按包晶反应生成. 由 EDS 分析结果可知熔覆层稀释区内 W 元素质量分数略高于 40%,该范围内的 Fe/W 元素质量比有利于 Fe_2W 的形成,由 XRD 结果也可以证实该白灰色细小颗粒相为 Fe_2W,其均匀分布于 α-Fe 固溶体中.

图 7c,d 分别为相同倍数下熔覆区上部和下部的显微组织. 可看出上部为灰色的粗大树枝状组织大致均匀的分布在灰黑色连续相之上,下部主要为灰色的短棒状组织同样分布在灰黑色连续相之上,粗大的树枝相和短棒相之间弥散分布着灰色的细小颗粒相,如图 7e. 由 EDS 结果可知熔覆区内 W 元素含量明显高于稀释区,其中树枝状晶粒所含 W 元素比例更高,结合 XRD 可以推断灰色的粗大树枝状晶粒和短棒状晶粒为 Fe_7W_6 相. 分析认为,合金熔池的主要成分为 W 和 Fe 元素. 随着熔覆层厚度增加,熔池逐渐远离基底材料,熔池中的 Fe 元素越来越少,而钨粉的输入量始终不变,致使熔池中 W 元素比例不断增大. 随着熔池快速冷却, 存在温度最高(1 637 ~ 1 190 ℃) 的 Fe_7W_6 相首先从溶液中按包晶反应凝固析出. 其首先以短棒状形式析出,其中一部分由于局部的能量不同和成分起伏会发展成为树枝状形态. 因此靠近熔覆区上层的区域由于 W 元素含量较高而形成了较多的粗大树枝状晶粒,而靠近下层的区域 W 元素含量相对较少,形成的 Fe_7W_6 相以短棒状为主. Fe_2W 由于具有与 Fe_7W_6 相类似的结构,除在极稳定的平衡条件下外,常会伴随着 Fe_7W_6 相持续生成. 因此熔池快速冷却条件下,析出温度较低的 Fe_2W(1 060 ℃) 将在周围的合金熔液中以细小的颗粒形式从初生的短棒状或树枝状 Fe_7W_6 晶间析出,弥散分布在 α-Fe 固溶体中,如图 7e 所示,Fe_2W 的组织结构与稀释区中的结构类似,如图 7f.

占熔覆层主体的熔覆区富含硬质 Fe_7W_6 相,因而使材料硬度得到了大幅提高,靠近熔覆层表层区域由于具有致密的枝晶组织,硬度提高尤为明显,而靠近下部的短棒状 Fe_7W_6 相尺寸相对较小,硬度略有下降. 稀释区组织主要为颗粒状的 Fe_2W,W 元素比例较低,因此该区域硬度值较熔覆区偏低. 而界面区的主要成份是 Fe 元素,仅有少量的 W 元素存在,硬度提高量较少. 可见熔覆层内 W 元素的含量对其硬度具有较大影响,随着熔覆层厚度的增加,熔覆层内部元素比例呈梯度变化,使得硬度值相应发生改变.

Fe_7W_6 化合物的形成不但能有效提高熔覆层的硬度,并且改变了材料的磨损形式. 这是由于熔覆层内部所形成的初生相 Fe_7W_6 具有较高的硬度,其作为增强相在磨损中形成硬质点,阻碍了磨损过程的进行,对基体起到了主要保护作用. 另一方面 Fe_7W_6 相之间分布的 α-Fe/Fe_2W 组织具有较好的塑性和韧性,对 Fe_7W_6 增强相起到支撑和附着的作用,也有利于提高熔覆层的耐磨性能.

4 结 论

(1) 采用同轴送粉激光熔覆方法,以纯钨粉末为熔覆材料,在 Q235A 钢表面制备了 Fe-W 合金涂层,涂层与基底冶金结合良好,无明显裂纹或气孔.

(2) 熔覆层主要由粗大的树枝状或短棒状 Fe_7W_6 增强相和弥散分布的细小颗粒状 Fe_2W 相组成,二者共同分布在 α-Fe 固溶体中.

(3) 熔覆层中的 Fe_7W_6 增强相对基体材料起到了主要的支撑和保护作用,显著提高了基材表面性能. 熔覆层的显微硬度平均为 700 HV,为基底 Q235A 钢的 3.5 倍,熔覆层耐磨性也成倍提高.

参考文献:

[1] Mazumder J, Dutta D, Kikuchi N, *et al*. Closed loop direct metal deposition: art to part [J]. Optics and Laser Engineering, 2000 (34): 397 - 414.

[2] 翟玉峰, 王新洪, 黄 坚. 激光熔覆 TiC-Mo2C 颗粒增强 Fe 基涂层的组织与性能 [J]. 中国激光, 2009, 36(12): 3287 - 3292.
Zhai Yufeng, Wang Xinhong, Huang Jian. Microstructure and properties of TiC-Mo2C particles reinforced Fe-based composite coatings produced by laser cladding [J]. Chinese Journal of Lasers, 2009, 36(12): 3287 - 3292.

[3] Manna I, Dutta Majumdar J, Ramesh Chandra B, *et al*. Laser surface cladding of Fe-B-C, Fe-B-Si and Fe-BC-Si-Al-C on plain carbon steel [J]. Surface and Coatings Technology, 2006, 201(1 - 2): 434 - 440.

[下转第 44 页]

1993, 11(增刊), 1 – 8.
Duan Liyu. The present situation and prospect of friction welding [J]. Journal of Northwestern Polytechnical University, 1993, 11 (supple): 1 – 8.

[2] 美国焊接学会. 焊接手册(第 2 卷) [M]. 北京: 机械工业出版社, 1986.

[3] Sluzalec A. Thermal effects in friction welding [J]. International Journal of Mechanical Sciences, 1990, 32(6): 467 – 478.

[4] Moal A, Massoni E. Finite element simulation of the inertia friction welding of two similar parts [J]. Engineering Computations, 1995, 12(6): 497 – 512.

[5] Soucail M, Moal A, Naze L, *et al*. Microstructural study and numerical simulation of inertia friction welding of astroloy [C] // 7th International Symposium on Superalloys, Seven Springs, USA, 1992: 847 – 856.

[6] 傅 莉, 刘小文, 鄢君辉, 等. 惯性摩擦焊接钢管焊合区热塑性变形参量场的数值分析 [J]. 机械科学与技术, 2000, 19(3): 339 – 440, 444.
Fu Li, Liu Xiaowen, Yan Junhui, *et al*. Numerical analysis on the coupled thermo-plastic deformation field during inertia friction welding of steel tube [J]. Mechanical Science and Technology, 2000, 19(3): 339 – 440, 444.

[7] 桂方亮, 张全忠, 张立文, 等. 几何参数对环件摩擦焊接轴向缩短量的影响 [J]. 材料科学与工艺, 2007, 15(5): 624 – 627.
Gui Fangliang, Zhang Quanzhong, Zhang Liwen, *et al*. The effects of geometric parameters on axial shortening of inertia friction weldment in ring form [J]. Materials Science and Technology, 2007, 15(5): 624 – 627.

[8] Zhang Liwen, Pei Jibin, Zhang Quanzhong, *et al*. The coupled fem analysis of the transient temperature field during inertia friction welding of GH4169 [J]. Acta Metallurgica Sinica (English Letters), 2007, 20(4): 301 – 306.

[9] Grant B, Preuss M, Withers P J, G, *et al*. Finite element process modelling of inertia friction welding advanced nickel-based superalloy [J]. Materials Science and Engineering A, 2009, 513 – 514: 366 – 375.

[10] 师昌绪, 李恒德, 周 廉. 材料科学与工程手册(上卷) [M]. 北京: 化学工业出版社, 2004.

[11] 安继儒. 中外常用金属材料手册 [M]. 西安: 陕西科学技术出版社, 2005.

[12] Demange J J, Prakash V, Pereira J M. Effects of material microstructure on blunt projectile penetration of a nickel-based super alloy [J]. International Journal of Impact Engineering, 2009, 36 (8): 1027 – 1043.

作者简介: 王非凡,男,1987 年出生,硕士. 主要从事摩擦焊接研究工作. 发表论文 1 篇. Email: wangifw@ hotmail. com

通讯作者: 李文亚,男,教授. Email: liwy@ nwpu. edu. cn

[上接第 40 页]

[4] 杜宝帅, 邹增大, 王新洪, 等. 激光熔覆原位自生 Fe-Ti-B 系复合涂层物相组织研究 [J]. 材料热处理学报, 2008, 29(5): 134 – 138.
Du Baoshuai, Zou Zengda, Wang Xinhong, *et al*. Investigation on phase constitunets and microstructure of in situ Fe-Ti-B composite coatings fabricated by laser cladding [J]. Transactions of Materials and Heat Treatment, 2008, 29(5): 134 – 138.

[5] 张 松, 张春华, 文效忠, 等. 2Cr13 钢表面激光熔覆 Co 基合金组织及其性能 [J]. 稀有金属材料与工程, 2001, 30(3): 220 – 223.
Zhang Song, Zhang Chunhua, Wen Xiaozhong, *et al*. Microstructure and performance of a laser clad Co-based alloy on 2Cr13 stainless steel [J]. Rare Metal Materials and Engineering, 2001, 30 (3): 220 – 223

[6] White J E. Development of oxidation resistant tungsten-base alloys [J]. AIAA. Journal, 1966(4): 307 – 312.

[7] Etemad G A. Oxidation and mechanical performance of tungsten at high temperatures and high pressures [J]. AIAA. Journal, 1966 (4): 1543 – 1548.

作者简介: 武 扬,男,1984 年出生,博士. 主要从事激光熔覆方面的科研工作. 发表论文 3 篇. Email: wuyang0203@ 163. com

通讯作者: 虞 钢,男,研究员,博士研究生导师. Email: gyu@ imech. ac. cn

methods applied in seam tracking.

Key words: image processing; seam tracking; centerline; linearity; the least-square method

Microstructure and properties of Fe-W composite coating by laser cladding WU Yang, YU Gang, HE Xiuli, NING Weijian (Key Laboratory of Mechanics in Advanced Manufacturing, Institute of Mechanics, Chinese Academy of Sciences, Beijing 100190, China). pp 37 - 40, 44

Abstract: An investigation of laser cladding Fe-W composite coating on Q235 steel was performed by injection of tungsten powder. The microstructure of the coating was analyzed with X-ray diffraction (XRD), optical microscope, scanning electron microscopy (SEM) and energy disperse spectroscopy (EDS). The microhardness and wear resistance were examined by hardness tester and abrading machine. The coating was metallurgically bonded with the substrate without visible crack or pore. The clad layer had a microstructure consisting of primary coarse dendrite or short stick Fe_7W_6 and fine isolated Fe_2W particles which uniformly dispersed in the α-Fe matrix. The average microhardness of the clad layer was approximately 700 HV which was 3.5 times greater than that of the Q235 substrate. The wear resistance was also obviously improved.

Key words: laser cladding; coaxial powder injection; Fe-W composite coating; microhardness; wear resistance

Numerical study on influence of axial pressure on inertia friction welding WANG Feifan, LI Wenya, CHEN Liang, LI Jinglong (State Key Laboratory of Solidfication Processing, Shanxi Key Laboratory of Friction Welding Technologies, Northwestern Polytechnical University, Xi'an 710072, China). pp 41 - 44

Abstract: A 2-D finite element model of inertia friction welding of GH4169 tubular was established based on the ABAQUS environment. The effect of axial pressure on the temperature field and axial upset of the joint was investigated by adopting the remeshing technique. The variations of joint temperature field under different axial pressures were also expounded. Moreover, according to the change of axial upset, the effect of axial pressure on the flash shape was analyzed. The results show that increasing axial pressure can significantly raise the conversion efficiency from flywheel kinetic energy to weld heat, shorten the time to high temperature quasi-steady state, and obtain flash shape. However, an extensively large pressure is negative to temperature field uniformity, which may result in bad stress concentration. At last, the pressure of 400 MPa is supposed to be a good parameter in this study.

Key words: inertia friction welding; axial pressure; temperature field; flash shape

Finite element modeling of residual stress in bonding interface of Ni-Cr/porcelain ZHU Song[1], ZHOU Zhenping[2], QIU Xiaoming[3] (1. College of Stomatology, Jilin University, Changchun 130021, China; 2. College of Machanical Science and Engineering, Jilin University, Changchun 130022, China; 3. College of Materials Science and Engineering, Jilin University, Changchun 130022, China). pp 45 - 48, 52

Abstract: The numerical value and distribution of residual stress in the bonding interface of Ni-Cr/porcelain and Ni-Cr/Ti/porcelain have been investigated by finite element method. The experimental results show that there is much difference in thermal expansion coefficient between Ni-Cr alloy and proclaim. Larger residual stress will be produced at the interface. Due to produced stress concentration at the corner resulted in edge effect, the maximal value of residual stress is 131 MPa, which appears at the Ni-Cr alloy/proclaim interface near proclaim side. The greater σ_z value appears in a narrow area on the near porcelain side. The greater shearing stress τ_{zx} value appears in the Ni-Cr/porcelain interface, and gradually decreases to Ni-Cr alloy and porcelain sides. Residual stress and distribution position of Ni-Cr/Ti/porcelain has been improved when using Ti interlayer comparing with the residual stress of Ni-Cr/porcelain interface. Inner stress between Ni-Cr alloy and porcelain has been released and the residual stress is transferred to Ti interlayer; The thickness of Ti interlayer has effects on residual stress, the σ_z of interface is increasing and shearing stress τ_{zx} is little different with the interlayer thickness increasing.

Key words: Ni-Cr alloy; porcelain; residual stress; finite element; Ti interlayer

Study on influence of CNT to nugget of aluminum alloy spot welding WANG Hao[1,2], LUO Zhen[1,2], ZHOU Linshu[1], ZHANG Di[1,2] (1. School of Materials Science and Engineering, Tianjin University, Tianjin 300072, China; 2. Tianjin Key Laboratory of Advanced Joining Technology, Tianjin University, Tianjin 300072, China). pp 49 - 52

Abstract: The process of aluminium alloy spot welding is widely used nowadays and the industry puts forward higher request in its properties and quality. The microstructure of aluminium alloy spot welding nuggets decides its macroscopic properties. In this paper, the microstructure of nugget was changed to enhance its properties and quality. Carbon nano-tube (CNT) was chosen as the addition of the aluminium alloy spot welding, and further analysis of the mechanical properties, microstructure and components of the welding spot of aluminium alloy. The results indicated that when the CNT was added in the aluminium alloy, the sizes of spot welding grain decreased significantly. The CNT distributed uniformly in the nuggets and it could increase the hardness and intensity significantly. The further analysis indicated that the carbon nano-tubes strengthening mechanism was mainly dislocation multiplication, transformation of load, constrained deformation and fine grain strengthening.

Key words: aluminum alloy; resistance spot welding; carbon nano-tube; model of strengthen theory

Microstructures and wear resistance of Ni-based PLA surfacing layer with introducing magnetic field LIU Zhengjun[1], LI Lecheng[1], ZONG Lin[1,2], SU Yunhai[1], SU Ming[1] (1. School of Material Science and Engineering, Shenyang University of Technology, Shenyang 110870, China; 2. School of Mechanical Engineering, Shenyang University of Chemical Technology, Shenyang 110142, China). pp 53 - 56

Abstract: Ni-based alloy was surfaced on low-carbon steel by plasma arc surfacing under DC transverse magnetic field. The hardness, wear resistance, microstructure and phase constitution of the surfacing layers were investigated via hardness and wear tests as well as SEM, EDS and XRD analysis. The influence of DC transverse magnetic field on the microstructures and wear resistance of the surfacing layer, the shape and amount of the hard phase were systematically studied. Furthermore, pre-